THEORETICAL STUDIES OF IMPORTANT PROCESSES IN PLANETARY AND COMET ATMOSPHERES

Semi-Annual Status Report

April 1, 1990 - October 31, 1990

NASA Grant NAGW 1404

Steven L. Guberman

Institute for Scientific Research

33 Bedford St., Suite 19A

Lexington, MA 02173

The NASA technical officer for this grant is

Dr. J. T. Bergstralh

Solar System Exploration Division, Code EL

NASA Headquarters, Washington, D. C. 20546

This is the fourth semi-annual progress report describing research on dissociative recombination reactions in planetary and comet atmospheres.

I. Introduction

In previous progress reports we have reported on the development of a computer program which determines dissociative recombination (DR) cross sections and rates using potential curves and electronic capture widths which have been calculated in this laboratory.[1,2,3] The program uses Multi-Channel Quantum Defect Theory (MQDT) to include excited Rydberg resonance levels in the DR cross section and rate calculations. In the current reporting period we have revised the program in order to calculate cross sections and rates for DR from excited ion vibrational levels. These cross sections and rates are very important in planetary ionospheres where it is well known that a substantial fraction of the molecular ions are vibrationally excited at high altitudes.[4] The laboratory determination of DR rates which are meaningful for planetary ionospheres is very difficult since one can generally not generate ions in specified vibrational levels or in the distributions found in planetary ionospheres. However, with a theoretical approach one can determine the rates for individual ion vibrational levels.

Each vibrational level of a molecular ion is the limit for an infinite series of Rydberg states. Above each ion vibrational level are Rydberg vibrational levels having higher ion levels as their series limit. These Rydberg vibrational levels are resonances, i.e. neutral states which are imbedded in the electron-molecular ion continuum. The states are illustrated in Fig. 1 which is taken from a manuscript currently in preparation.[5] A

single neutral Rydberg state with principal quantum number n=6 is shown with a dotted line. At electron energy ε, dissociative recombination occurs into the repulsive $^1\Sigma_u^+$ state. However at energy ε', the n=6,v=5 state can be populated. At energy ε', this Rydberg level causes an abrupt perturbation in the cross section for DR because of interference between capture into the Rydberg level and capture into the repulsive dissociative state. This latter process is referred to as indirect recombination. The process in which the Rydberg levels are excluded and recombination goes from the entrance channel to the repulsive state is called direct recombination. The full DR process, i.e. both direct and indirect recombination, is the process of importance for planetary atmospheres. However, in the discussion below, we include the direct process in order to assess the role of the resonances.

II. DR Cross Sections and Rates

These ideas are illustrated here with the new results for DR from excited ion vibrational levels of O_2^+ into the $^1\Sigma_u^+$ dissociative state (as shown in Fig. 1) which leads to $O(^1S) + O(^1D)$. Fig.2 shows the calculated DR cross section for the v=1 ion vibrational level for electron energies up to 1eV. The cross section that has no structure is the "direct" DR cross section in which the resonance states are excluded. The direct cross section shows a sharp drop near 0.22eV where the v=2 level of the ion becomes accessible. At this energy the incoming electron can be ejected leaving the ion in a new vibrational state, v=2. This process causes a sudden drop in the DR cross section and corresponds to vibrational excitation assisted by the neutral repulsive state. Three smaller drops are discernible at higher energies corresponding to the v=3,4 and 5 ion levels. The cross section curve showing considerable structure is the full DR curve which includes the Rydberg

resonances. Before each of the v=2,3,4,5 ion levels there is a thick cluster of Rydberg levels corresponding to the series which has its limit at each ion level. In the calculations we include levels up to n=20. The first resonance shown in Fig.2 at 0.03eV corresponds to the n=9,v=2 Rydberg level followed by the n=10,v=2 level at 0.07eV. Both these resonances have a similar shape, however n=10 is more contracted. The resonances get narrower as n increases. Note that at very low electron energies the cross section which includes the resonances (the full cross section) is below the cross section without the resonances. This difference is due to the n=8,v=2 resonance which is below the v=1 level. While this state is discrete with respect to the v=2 electron-ion continuum it has a wing which extends above threshold. The n=8,v=2 resonance has a similar shape to that for n=9,v=2 and the high energy wing of the n=8 resonance decreases the cross section below the direct cross section.

Fig.3 has a plot of the DR probability for v=1. The DR probability is the cross section divided by the maximum allowed cross section at that electron energy. The probability has a maximum value of 1.0 and has the electron energy dependence of the cross section removed. This linear plot shows more of the complex detail in the cross section due to the resonances. Once again, the plot without structure is the direct cross section. The sharp breaks in the direct cross section due to the opening of new autoionization channels is readily apparent. Note that at certain "magic" energies the probability can be quite high.

Since there are more dips than peaks in Fig.'s 2 and 3 one would expect the indirect DR rate to be lower than the rate without the resonances. This is indeed the case as shown in Fig. 4 where the lower curve is the full DR rate and the upper curve is for direct DR only. The rate at 300K is

$5.2 \times 10^{-9} cm^3/sec$.

The MQDT method used for the calculation of cross sections and rates includes the interactions between all entrance and exit channels. In addition to DR, another exit channel is vibrational deexcitation in which the incoming electron is captured into the dissociative state but prior to dissociation the electron is emitted leaving the ion in a lower vibrational level. The intermediate neutral repulsive state can "assist" this process leading to a higher rate than in the absence of the repulsive state. The cross section for vibrational deexcitation from v=1 to v=0 is shown in Fig.5. The same resonances discussed earlier for DR enter the deexcitation cross section but with slightly different shapes. Note that in this case the cross sections with the Rydberg resonances included is considerably greater than the cross sections without the Rydberg resonances. As a result, the indirect rate for this process, shown in Fig.6 is above the direct rate. The full rate at 300K is $1.2 \times 10^{-10} cm^3/sec$.

Fig.'s 7-13 show similar results for the v=2 ion level. The first resonance here near 0.03eV is due to the Rydberg n=9,v=3 level. The next resonance is due to n=10,v=3 near .07eV but its shape is distorted by interference with n=4,v=8. Fig. 8 shows the probability plot where one can clearly discern 4 dense clusters of resonances just below the v=3, 4, 5, and 6 levels of the ion. As for v=1, the resonances exhibit more dips than peaks and the full DR rate (shown as the bottom curve in Fig.9) is below the direct DR rate. The full DR rate at 300K is $2.1 \times 10^{-8} cm^3/sec$.

For the v=2 ion level there are now two channels for vibrational deexcitation, v=0 and v=1. The cross section for the v=2 to v=0 channel is shown in Fig.10. Note that the n=9,v=3 resonance has a different shape in Fig.10 compared to Fig.7. The indirect rate for the 2-0 process is the upper

curve in Fig.11 and is similar to the direct rate except at high electron temperatures. At 300K, the full 2-0 rate is $2.0 \times 10^{-10} cm^3/sec$. Fig. 12 shows the 2-1 deexcitation process is about a factor of 8 larger than that for 2-0 at 0.01eV and the general resonance structure of the cross section is similar to that for 2-0. The indirect 2-1 deexcitation process is the upper curve at all temperatures shown in Fig.13. However, for temperatures below 300K, the two rates are nearly indistinguishable. At 300K the 2-1 process has a rate of $1.3 \times 10^{-9} cm^3/sec$.

The total deexcitation rates must include other channels in addition to the $^1\Sigma_u^+$ channel reported here. The calculation of rates along these other channels is in progress.

III. References

1. S. L. Guberman, Nature 327, 408 (1987).

2. S. L. Guberman, Planet. Space Sci. 36, 47 (1988).

3. S. L. Guberman, Ab Initio Studies of Dissociative Recombination, in Dissociative Recombination: Theory, Experiment, and Applications, ed. by J. B. A. Mitchell and S. L. Guberman (World Scientific, Singapore, 1989), p.45.

4. J. L. Fox, Planet. Space Sci. 34, 1241 (1986).

5. S. L. Guberman and A. Giusti, The Generation of $O(^1S)$ from the Dissociative Recombination of O_2^+, in preparation.

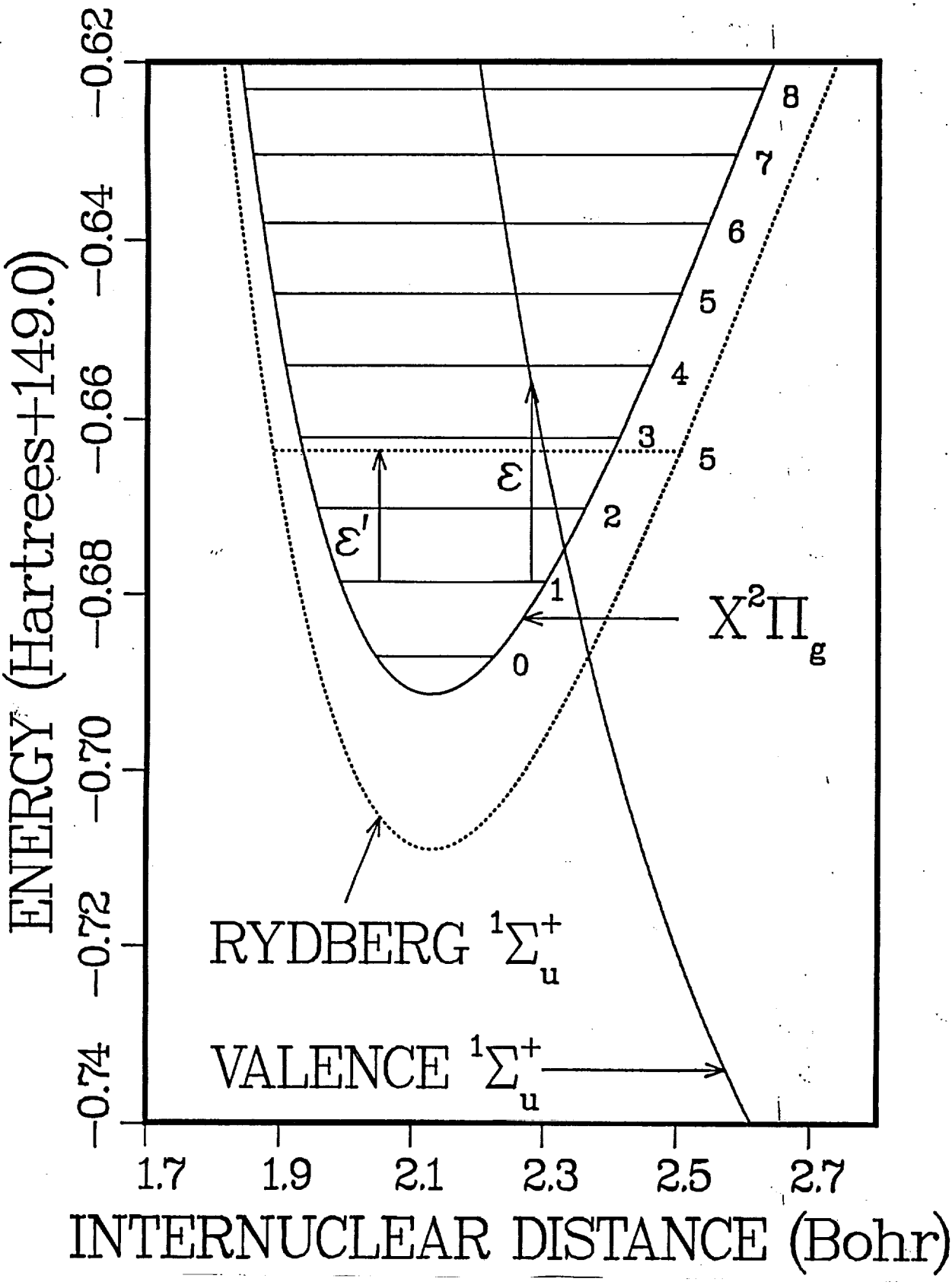

Figure 1. The dissociative $^1\Sigma_u^+$ state and ion potential are shown as solid lines. The dotted line is the n=6 Rydberg state.

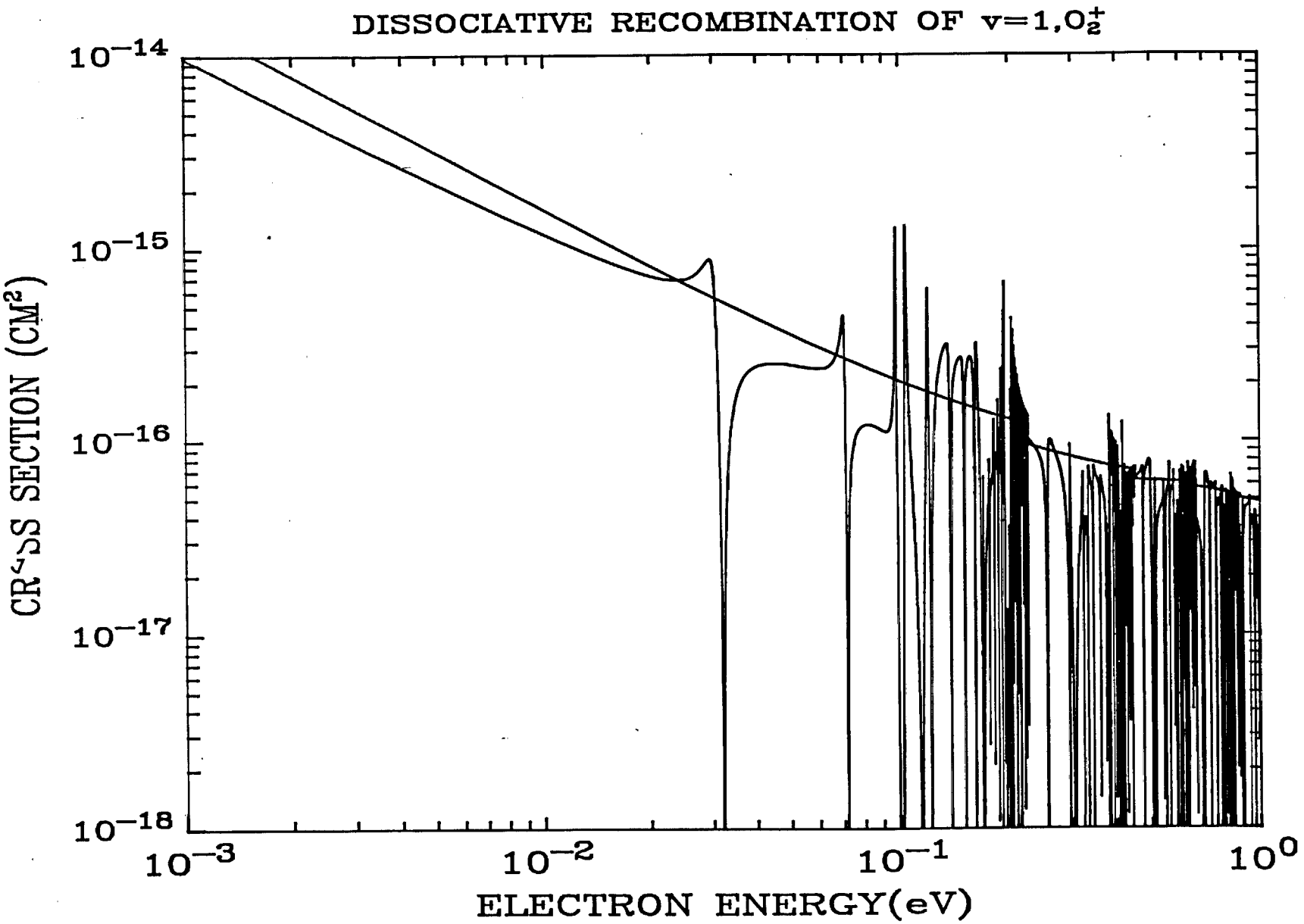

Figure 2. The direct and full DR cross section from the v=1 ion level.

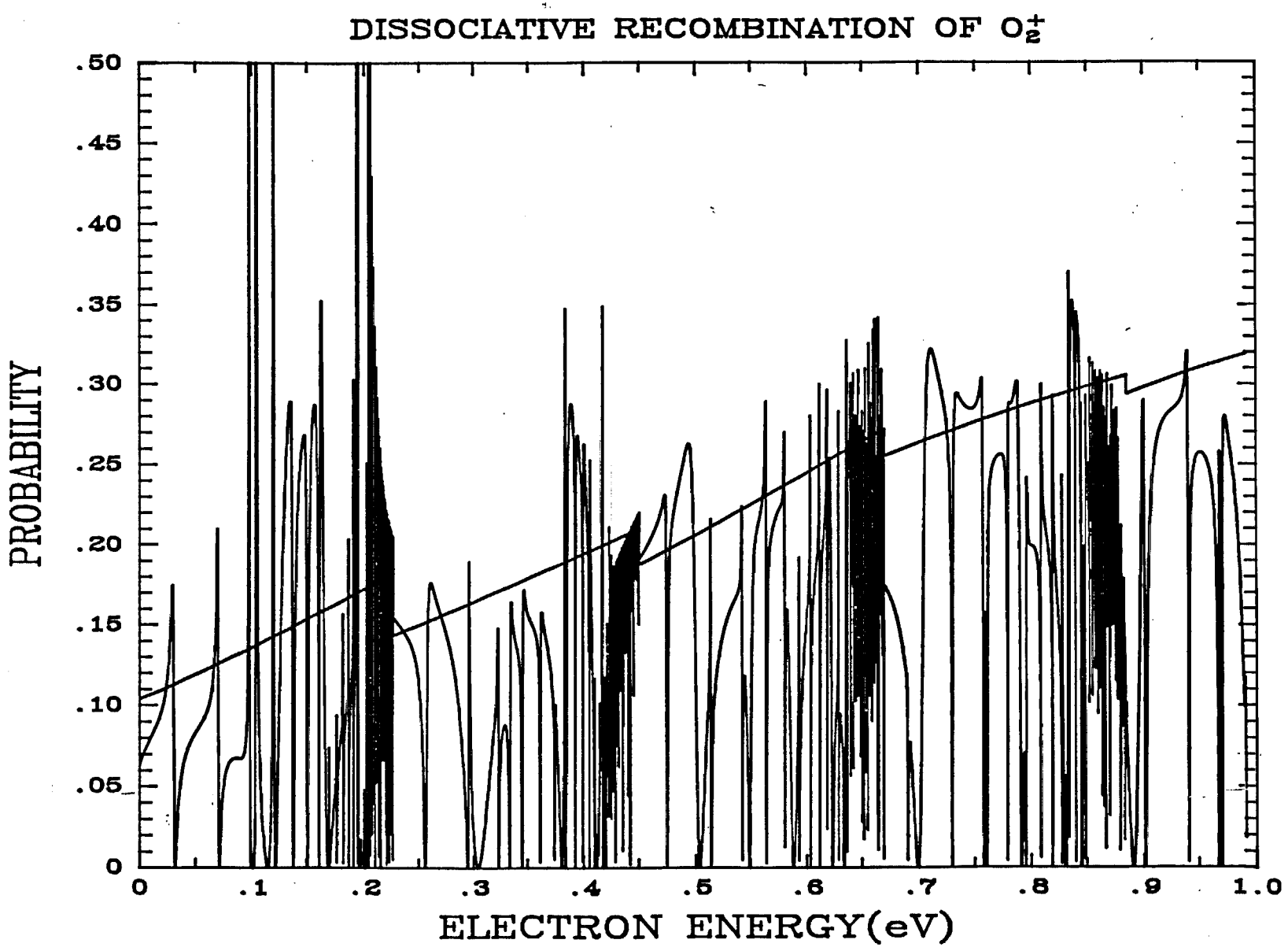

Figure 3. The probability for DR from v=1 is shown for both the full and direct cross sections.

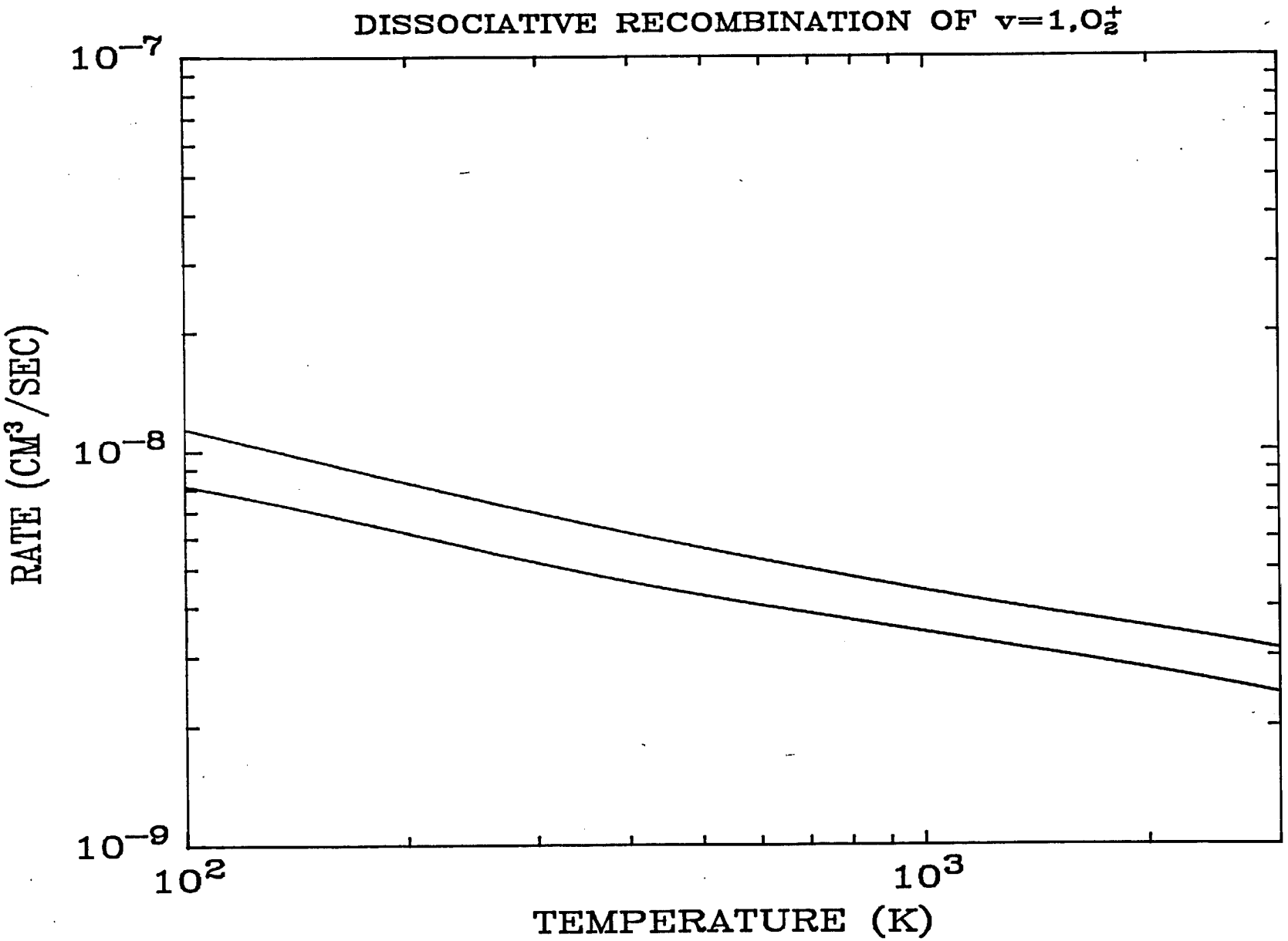

Figure 4. The full and direct rates for DR of the v=1 ion level are the lower and upper curves respectively.

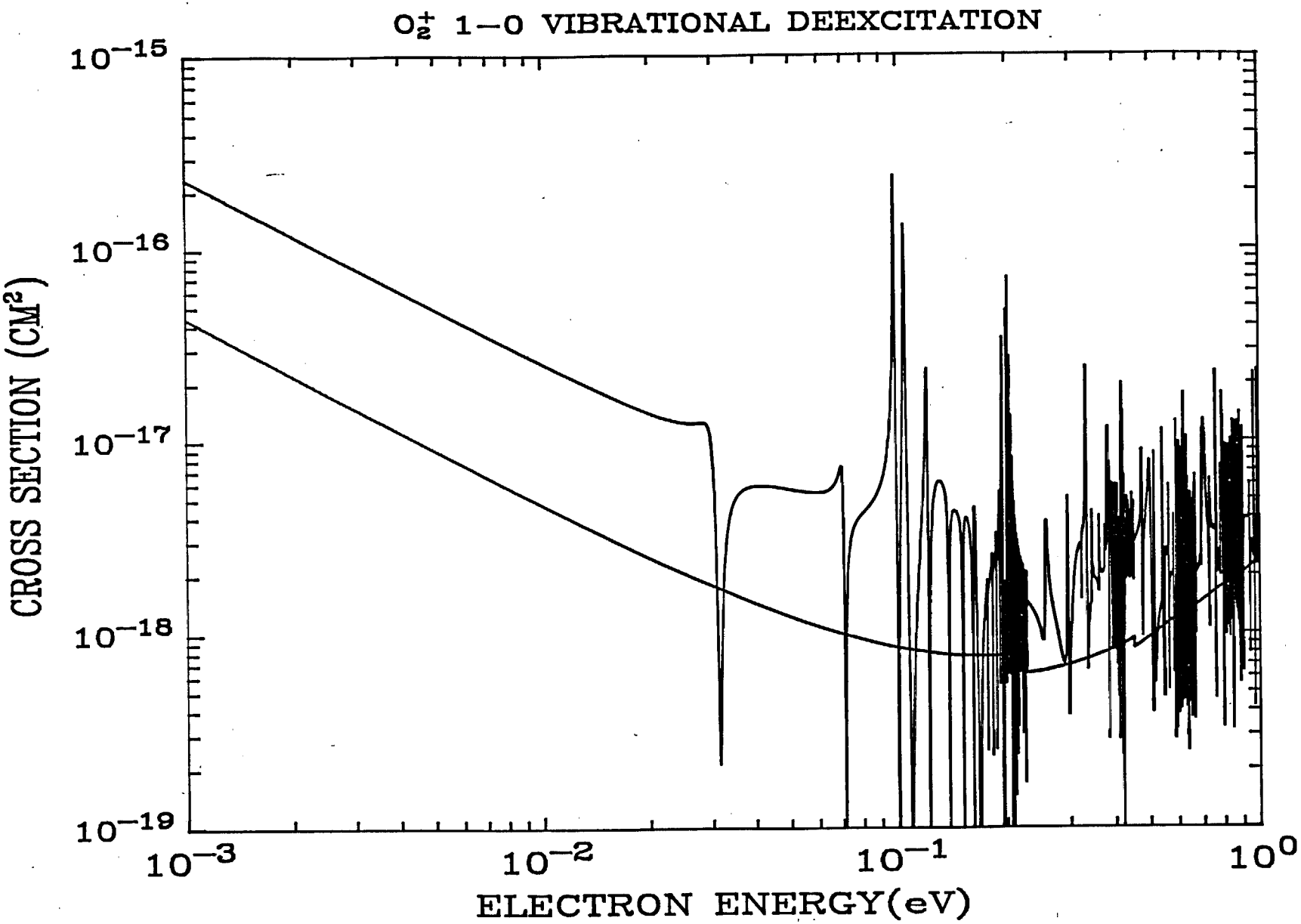

Figure 5. The full and direct 1-0 vibrational deexcitation cross sections.

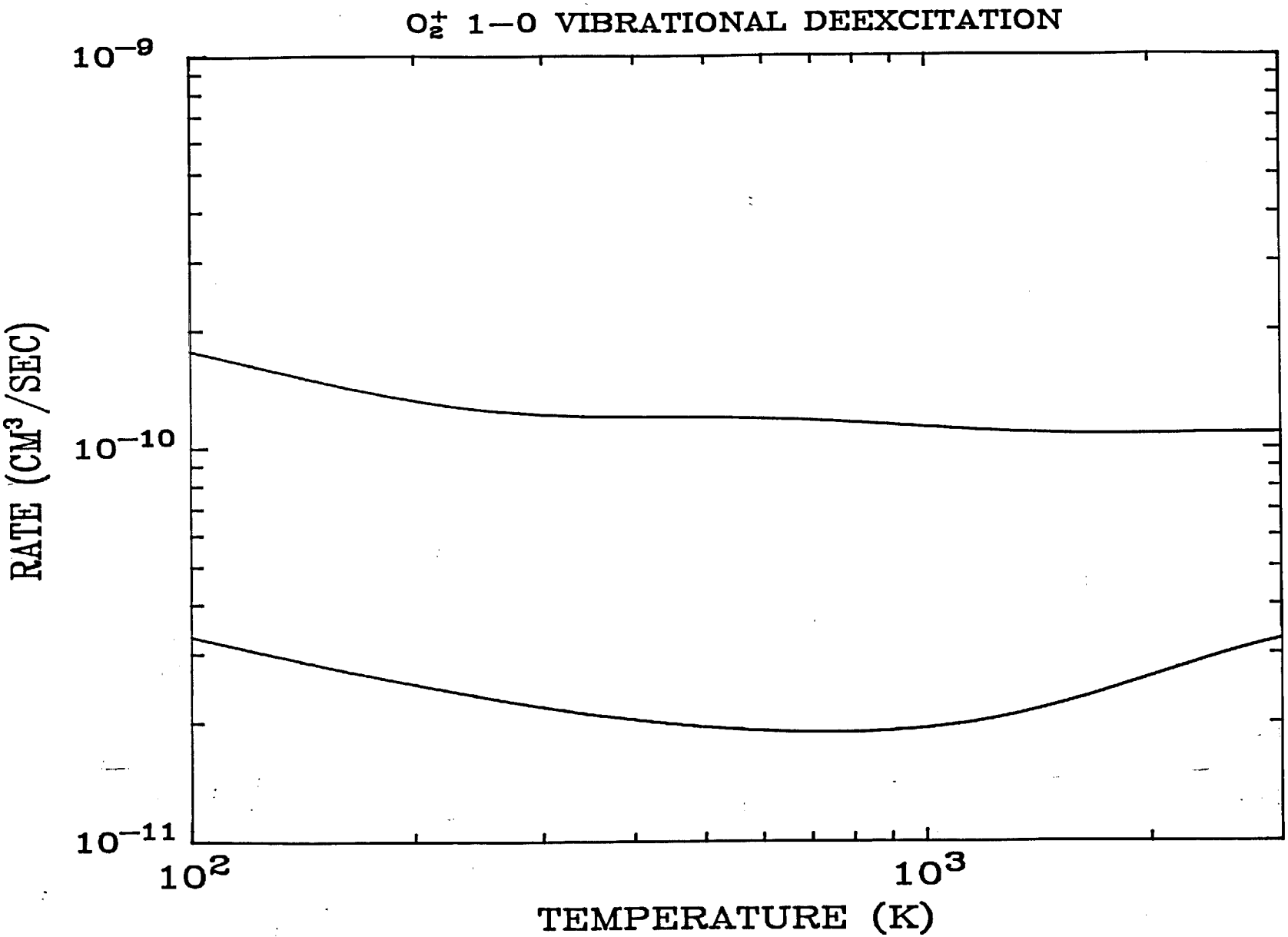

Figure 6. The full and direct 1-0 vibrational deexcitation rates are shown as the upper and lower curves respectively.

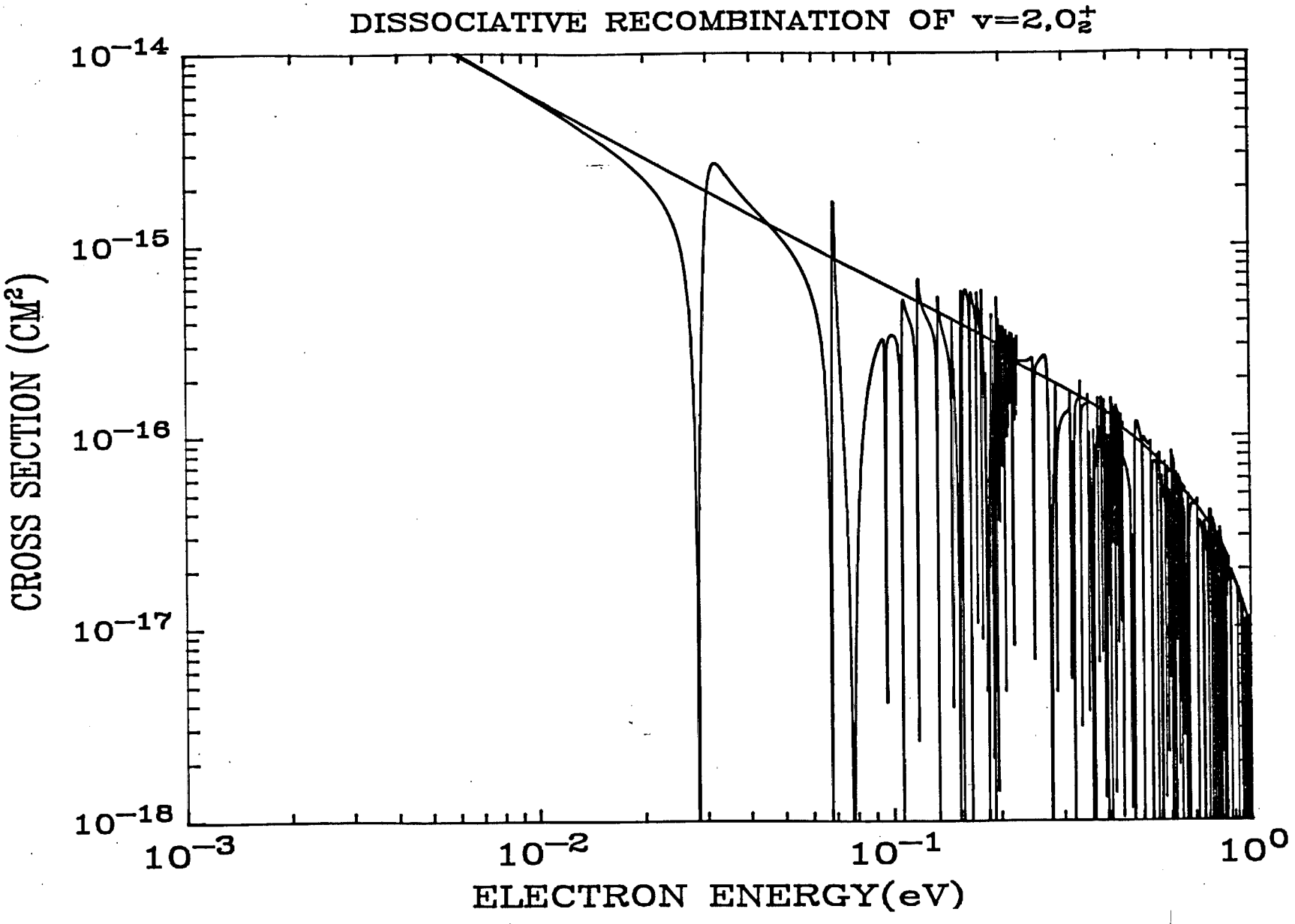

Figure 7. The direct and full DR cross section from the v=2 ion level.

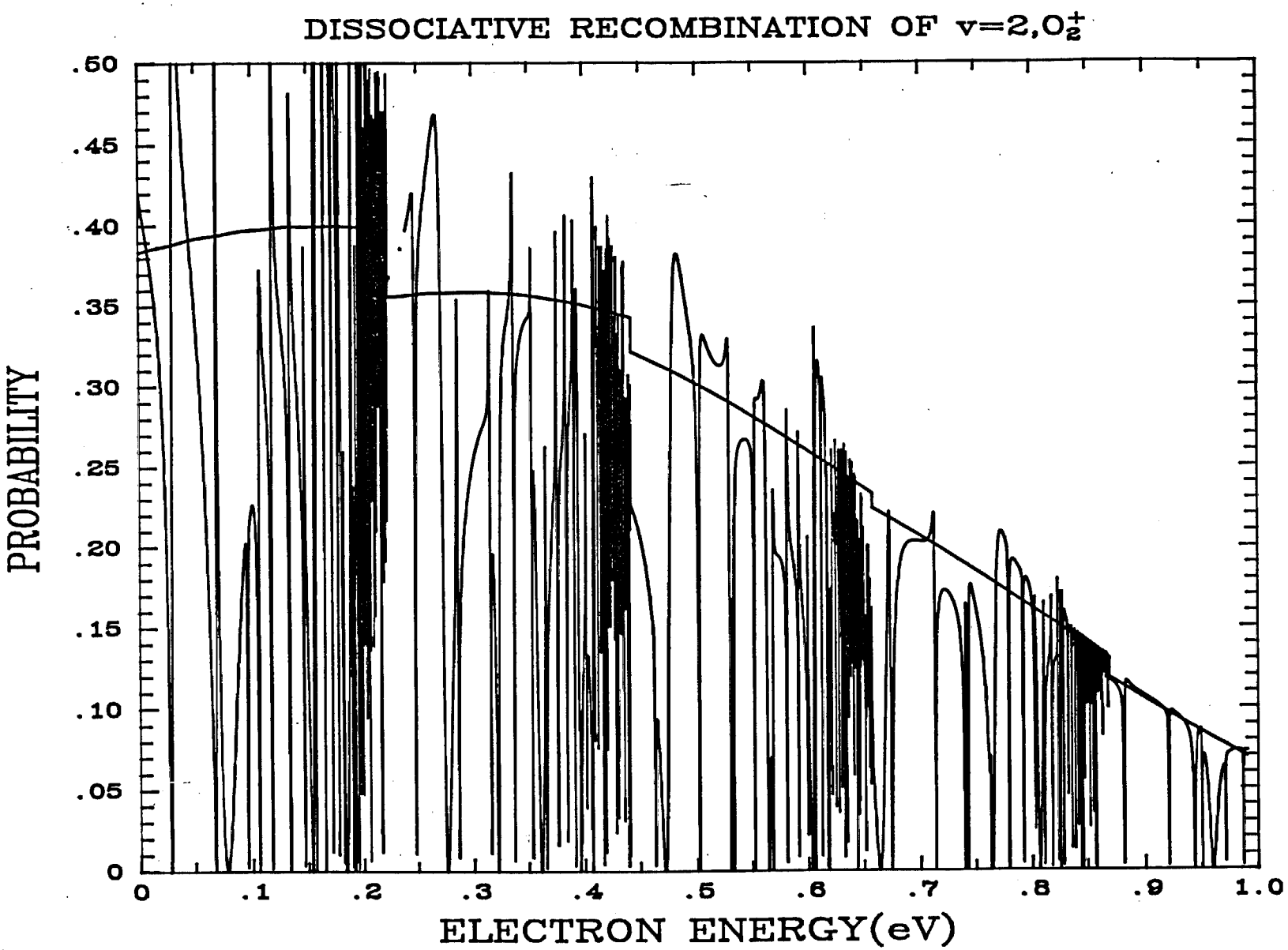

Figure 8. The probability for DR from v=2 is shown for both the full and direct cross sections.

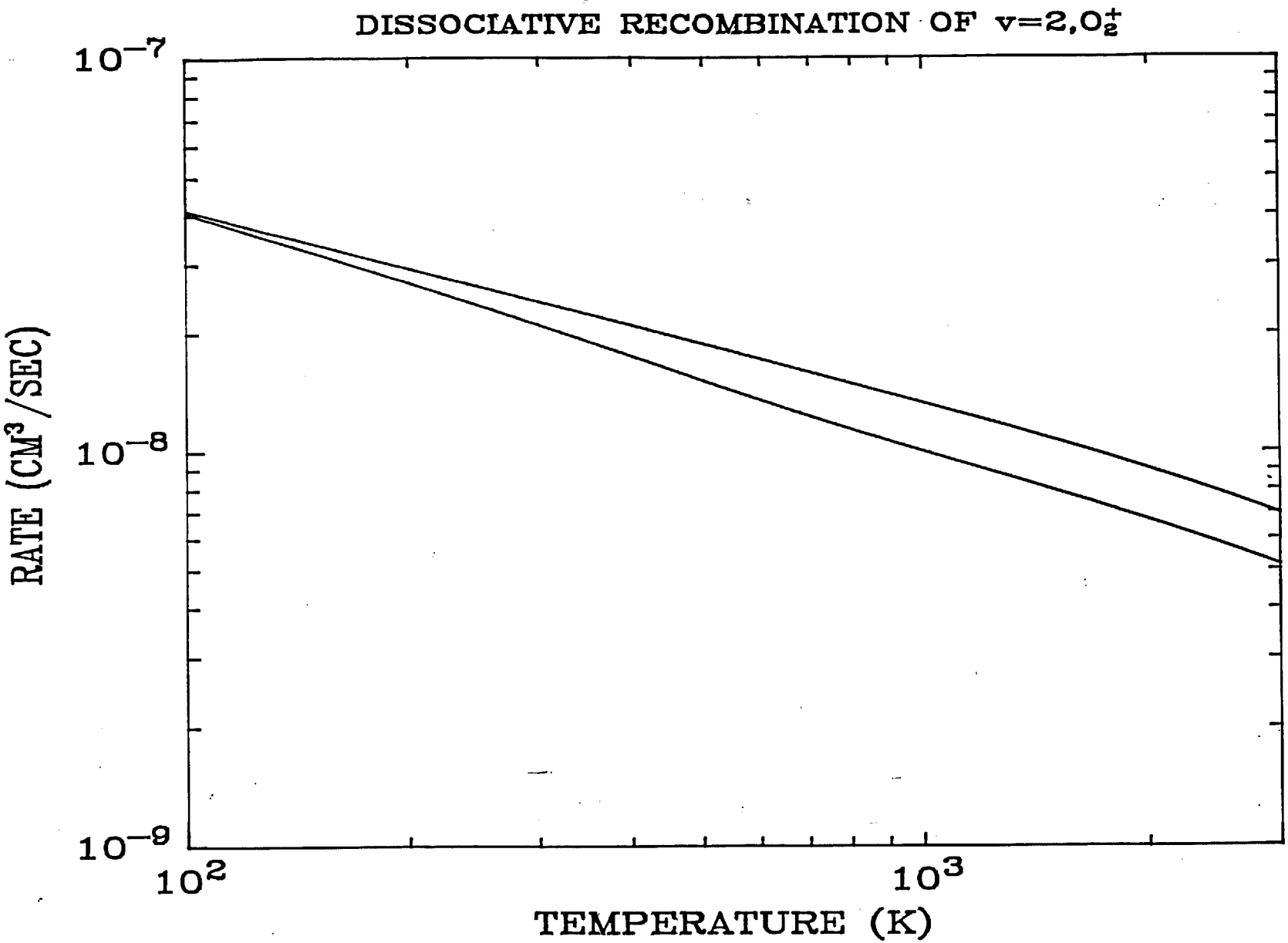

Figure 9. The full and direct rates for DR of the v=2 ion level are the lower and upper curves respectively.

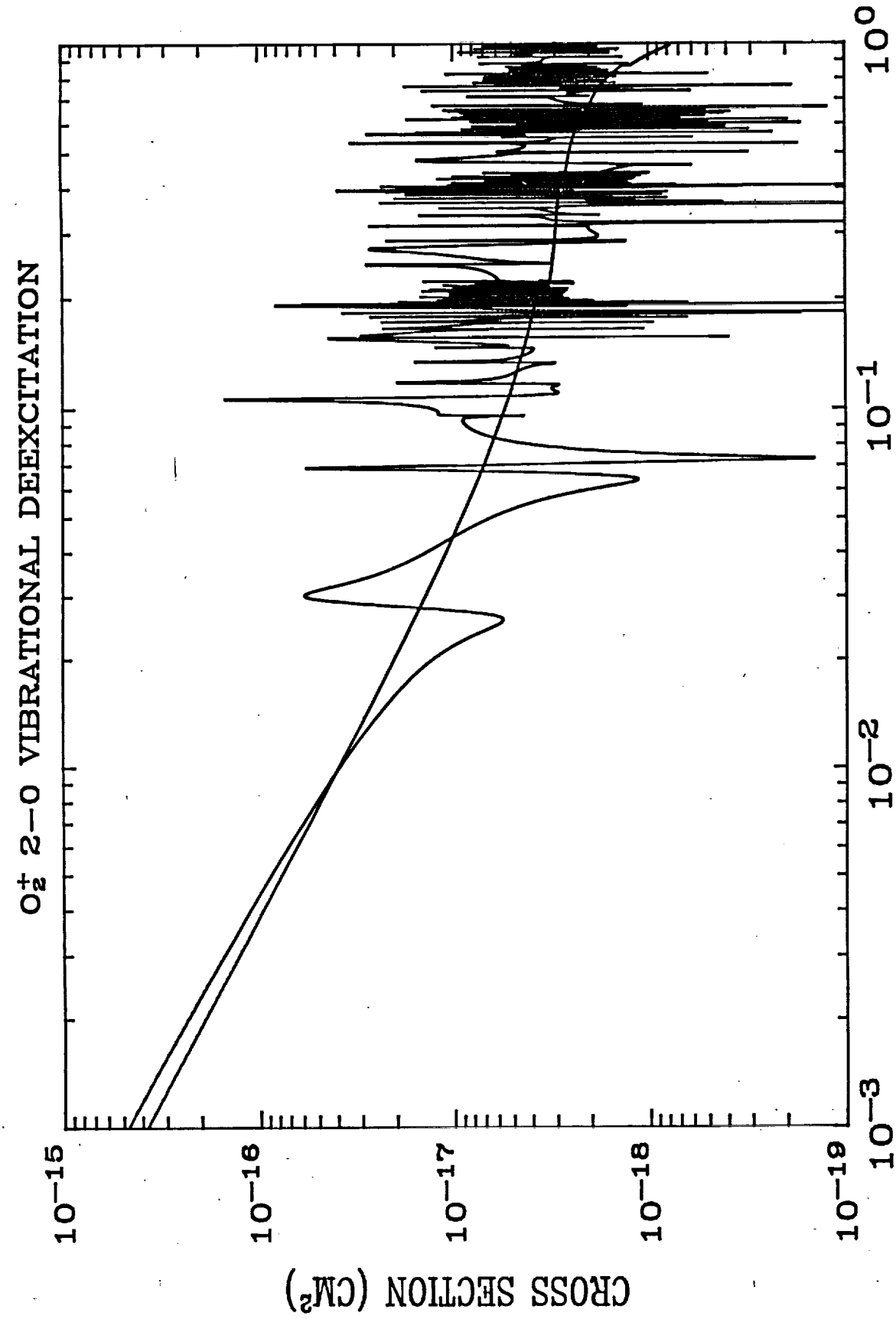

Figure 10. The full and direct 2-0 vibrational deexcitation cross sections.

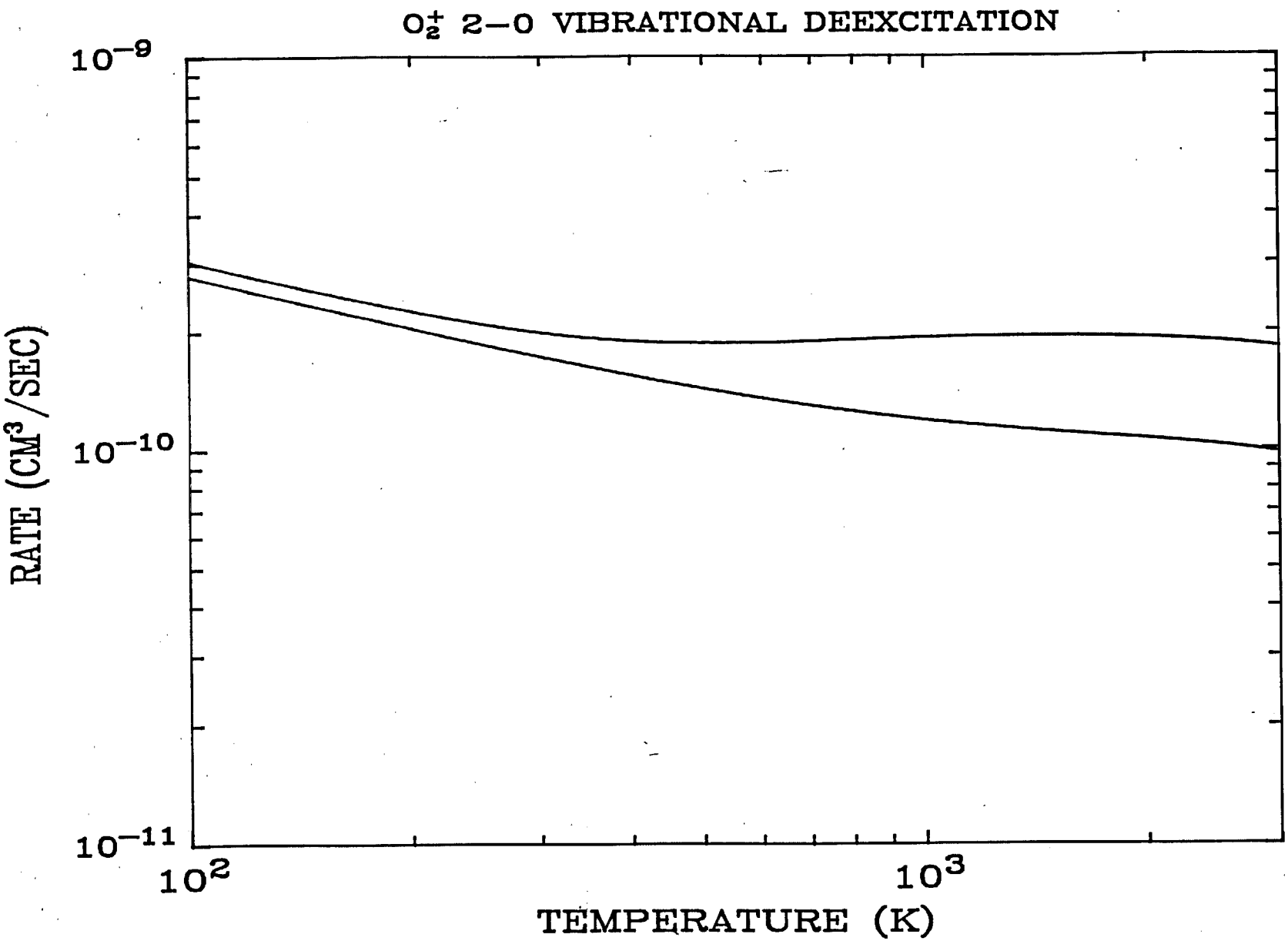

Figure 11. The full and direct 2-0 vibrational deexcitation rates are shown as the upper and lower curves respectively.

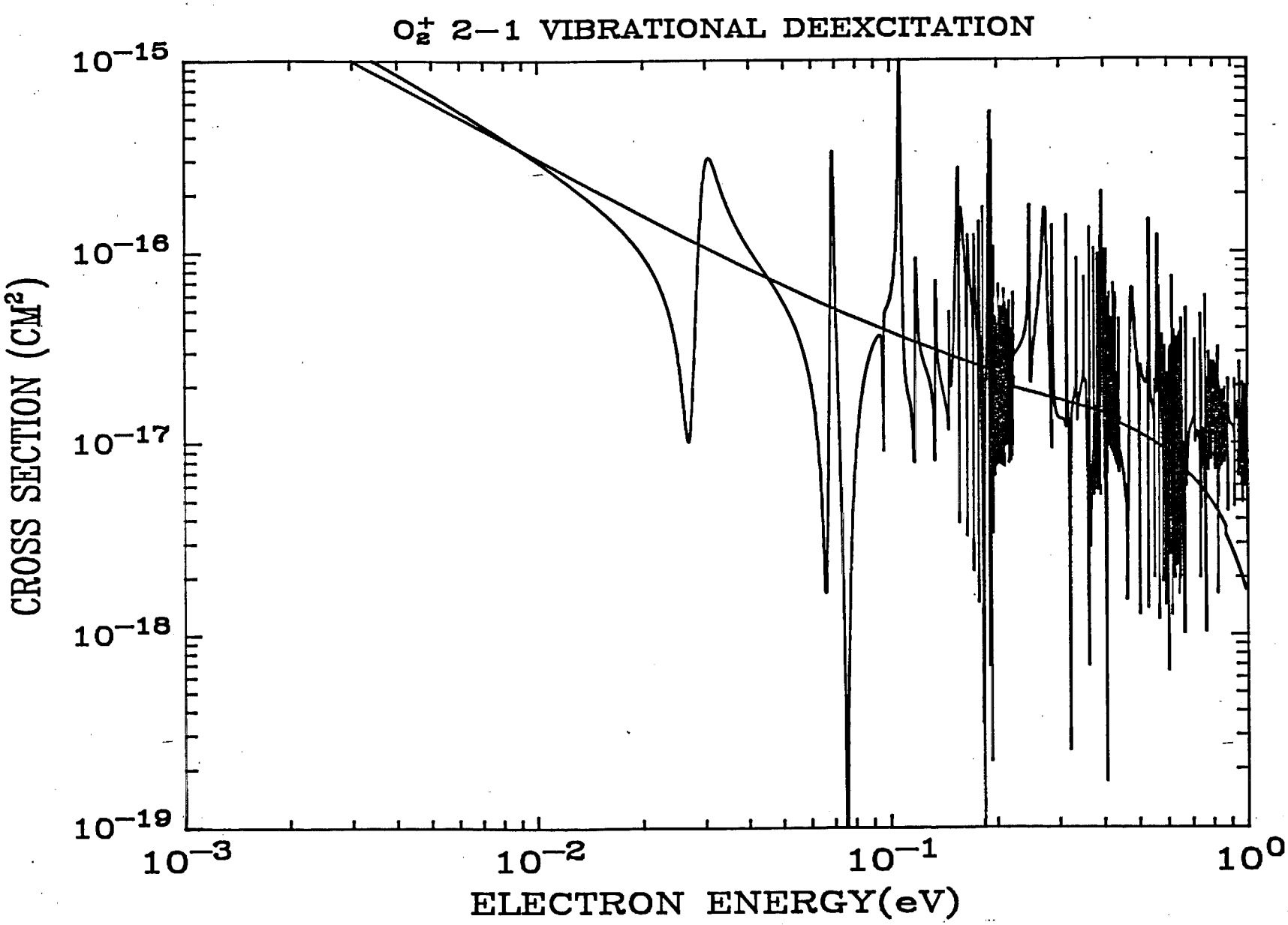

Figure 12. The full and direct 2-1 vibrational deexcitation cross sections.

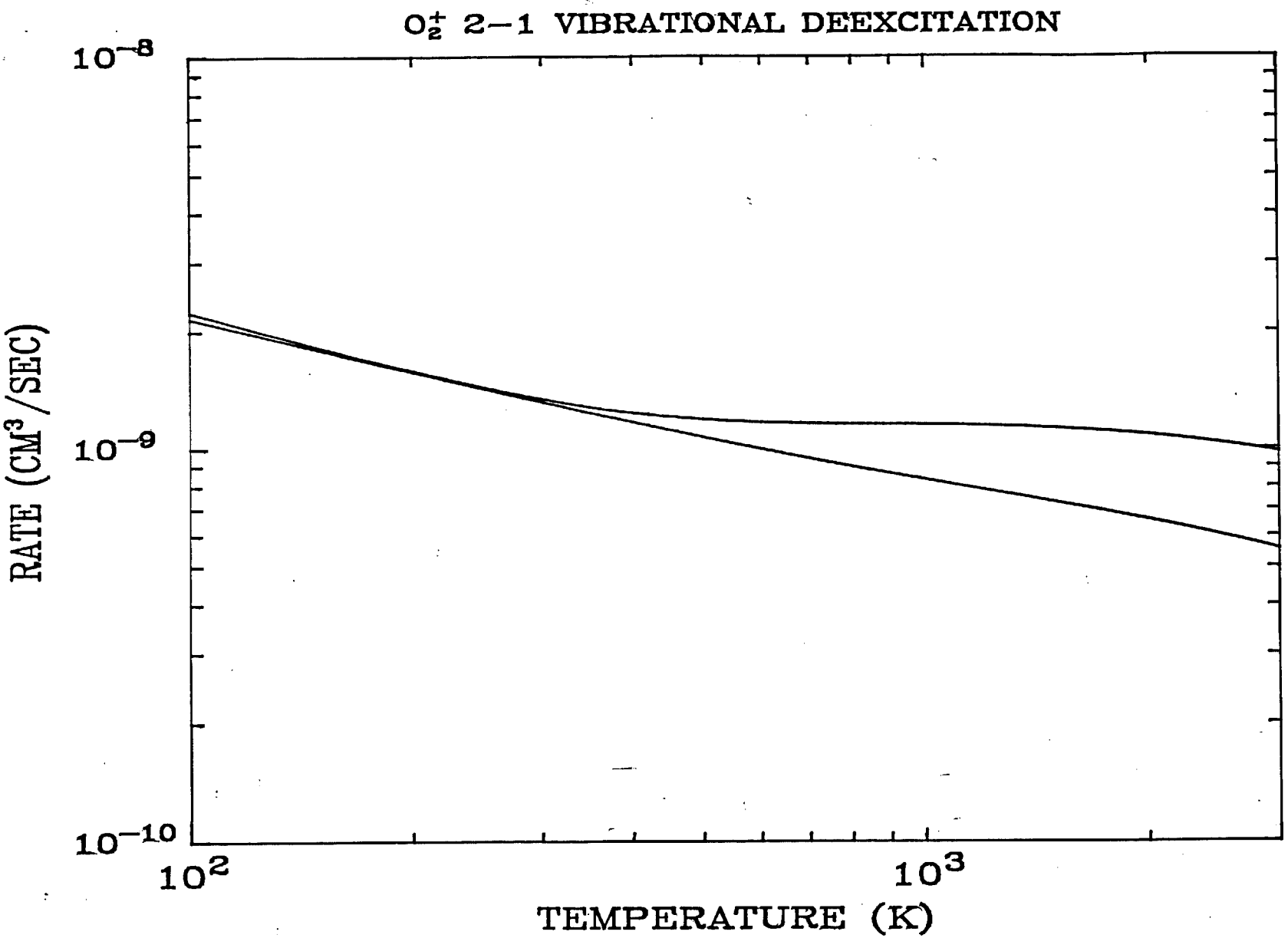

Figure 13. The full and direct 2-1 vibrational deexcitation rates are shown as the upper and lower curves respectively.